

VIII Inversion layers

Evgeni Fedorovich

8.1. Introduction

Dealing with diffusion and transport processes in atmospheric mesoscale flow fields one often comes across the situations when these processes take place within so-called atmospheric inversion layers, namely the layers characterized by the increase of the absolute temperature with height. In the course of the diurnal evolution of the atmospheric planetary boundary layer the two most typical examples of the sublayers with the inverse temperature gradient can be observed.

The first one is the stable layer capping the convectively mixed layer (ML) which develops over the heated underlying surface at the daytime and is driven by the positive buoyancy flux from the ground. Strictly speaking, the capping layer is not always strong enough to be classified as a temperature inversion. Still, it is commonly called the capping inversion layer (IL), or capping inversion. Stably stratified inversion layer acts as a lid to the buoyant thermals rising within the mixed layer. The process of interaction between the thermals and the capping inversion is characterized by the entrainment, or mixing down, the less turbulent air from above into the growing mixed layer. That is why the inversion layer in this case is called also the entrainment zone, regardless that the region with inverse absolute temperature gradients may occupy only the part of the layer where entrainment takes place.

The second example is the stable boundary layer (SBL), also called the nocturnal boundary layer, which usually originates at night, where the buoyancy flux at the surface is negative. Like in the capping inversion, in the nocturnal boundary layer vertical transport and diffusion are suppressed by the buoyancy forces. Therefore the turbulence in the stable boundary layer is usually weak and sporadic. The top of SBL is not very well-pronounced and can be defined in most cases merely as the height where turbulence intensity is a small fraction of the surface value. Sometimes SBL can also form during the day, for example when the warm air advection over a cool surface occurs.

Both inversion layers, the one which is capping the convectively mixed layer (elevated inversion), and the surface-based stable (nocturnal) layer, will be subjected to our consideration. We shall briefly discuss the phenomenology of these layers (for details see Stull, 1988), and present model approaches to their description.

8.2. Capping inversion

8.2.1. Characteristics and structure. A convective boundary layer driven by temperature and moisture fluxes at the ground commonly develops during the daytime over land surface. Its growth occurs on the background of stable stratification. Between the well-mixed layer adjacent to the surface and the quiescent layer, there is the capping inversion with strong stable density stratification (Figure 8.1). The inversion (entrainment) layer can be quite thick - averaging about 40% of the depth of the mixed layer. Buoyant thermals rising within the mixed layer overshoot into the capping stable air before sinking back into the ML, and their height of maximum rise defines the top of the entrainment zone. The bottom of entrainment layer is less well defined because there is no sharp demarcation (Nelson et al., 1989). Usually it is taken as that altitude where some small fraction of the air in the horizontal plane has free-atmosphere air characteristics.

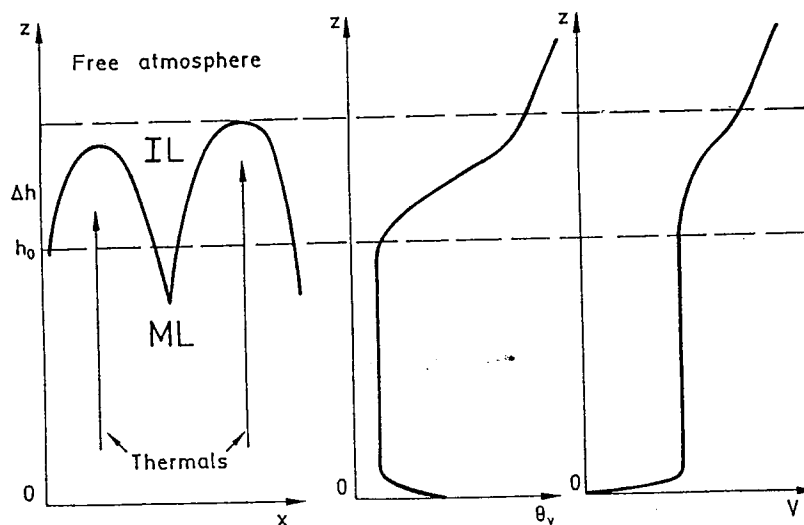


Figure 8.1. Schematic pattern of the capping inversion layer structure. After Stull (1988).

Sharp temperature gradients in the inversion layer are accompanied by substantial changes with height of other meteorological variables, for instance, wind speed and moisture. Pollutants emitted from the sources located within the ML are not able to penetrate into the free atmosphere due to the resistance caused by the static stability in the inversion layer. Trapping of pollutants below the elevated inversion is rather common feature of the convective boundary layer.

The entrainment zone essentially consists of turbulent thermals imbedded within non-turbulent free-atmosphere air. In addition to the large-scale motions associated with the thermals a variety of smaller scale motions exists in the entrainment layer. The latter ones only to small extent contribute to the ML air dispersion from thermals into the free atmosphere.

Kelvin-Helmholtz waves generated in the stably stratified environment of inversion is an important mechanism influencing the entrainment. On the largest scale these waves have the wavelength of the order inversion layer depth. They break, form turbulent spots, and thus contribute to the entrainment. On the smaller scales Kelvin-Helmholtz waves can originate along the top boundary of the thermal. Such short waves appear and decay into turbulence within few minutes. They stipulate the erosion of thermals, but their contribution to overall entrainment is rather small.

Penetration of thermals into the stably stratified air causes also the excitation of gravity waves in the free atmosphere aloft. Propagating at different angles away from the thermals these waves drain kinetic energy from the inversion layer.

In many instances the buoyancy production of turbulent kinetic energy in convective boundary layer considerably dominates over its production due to velocity shear, so the layer can be taken as shear-free. We shall consider one parameterized model for the capping inversion structure corresponding to this case, recently developed by the author in co-operation with Dr. Dmitrii Mironov from ICSC - World Laboratory, Erice, Italy.

8.2.2. Modelling the capping inversion structure. Physical quantity named *buoyancy* can be introduced for characterising the dense difference between the air particle and the surrounding air, and hence the ability of an air particle to rise. Buoyancy is defined as $b = g(\rho_0 - \rho) / \rho_0$, where ρ is the density, ρ_0 is the reference density, and g is the acceleration due to gravity; or, in terms of the virtual potential temperature, θ_v , as $b = g(\theta_v - \theta_{v0}) / \theta_{v0}$, where θ_{v0} is the reference value of θ_v . The air of rising thermals is warmer and less dense than the ambient ML air and therefore thermals possess positive buoyancy.

When horizontal averages of buoyancy are calculated from aircraft or lidar measurements data, the resulting buoyancy profile exhibits a smooth behaviour within the inversion layer (Figure 8.2). In the lower part of inversion, the mean buoyancy departs from the value characteristic of the mixed layer (where it is nearly uniform with height), higher on buoyancy sharply increases, reaching its maximum gradient at the height usually close to the middle of the layer, and then matches with the free-atmosphere buoyancy profile.

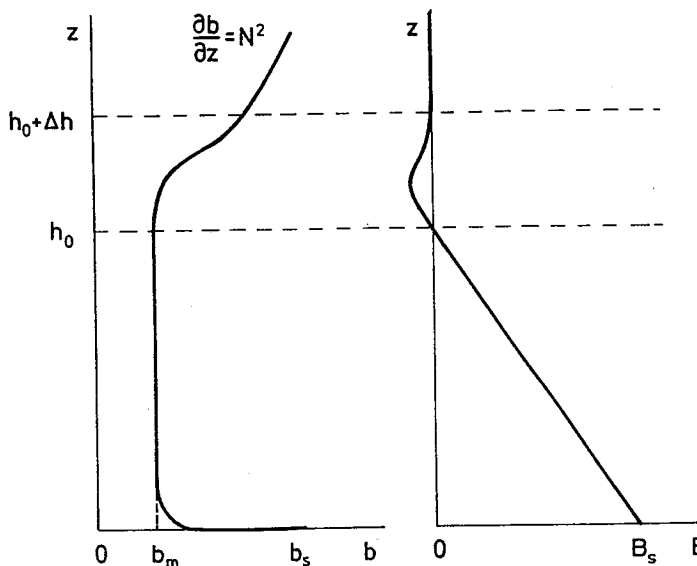


Figure 8.2. Vertical profiles of buoyancy and turbulent buoyancy flux in the convective boundary layer.

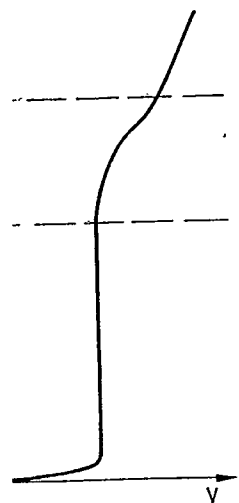
The vertical turbulent buoyancy flux decreases linearly with height in the main part of the mixed layer. Its zero crossing level roughly coincides with the bottom of the inversion layer. Being negative all over this layer, buoyancy flux reaches its minimum value within the entrainment zone and vanishes towards its upper boundary. Hence the alternative definition of the entrainment zone is that region where the buoyancy flux is negative.

We simplify the discussion by considering a horizontally homogeneous boundary layer without large scale subsidence, assuming that with the development of convection the vertical buoyancy profile $b(z,t)$ keeps the following form:

$$b = \begin{cases} b_m & \text{at } 0 \leq z \leq h_0, \\ b_m + \Delta b F(\zeta, G) & \text{at } h_0 \leq z \leq h_0 + \Delta h, \\ b_m + \Delta b + N^2(z - h_0 - \Delta h) & \text{at } h_0 + \Delta h \leq z. \end{cases} \quad (8.1)$$

Here $b_m(t)$ is the ML value of buoyancy, $h_0(t)$ is the ML depth, $\Delta h(t)$ is the depth of the inversion layer (IL), $\Delta b(t)$ is the buoyancy increment across IL, $N = \sqrt{\frac{\partial b}{\partial z}}$ is the buoyancy frequency in the free atmosphere, F is function of dimensionless co-ordinate $\zeta = (z - h_0) / \Delta h$ and stratification parameter $G = N^2 \Delta h / \Delta b$.

To provide for the continuity of the buoyancy profile at the boundaries of the IL we impose the following conditions on $F(\zeta, G)$:



structure. After Stull (1988).

panied by substantial changes in wind speed and moisture. The air is not able to penetrate into the stable layer in the inversion layer. Another common feature of the

thermals imbedded within the motions associated with the entrainment layer. The latter ones are entrained from thermals into the free

environment of inversion is an important scale these waves have the form of turbulent spots, and thus Kelvin-Helmholtz waves can originate and decay into turbulence due to their contribution to overall

also the excitation of gravity waves away from the thermals

kinetic energy in convective boundary layer to velocity shear, so the layer is often modeled for the capping layer developed by the author in laboratory, Erice, Italy.

Physical quantity named buoyancy is the force per unit mass on a particle of air to rise. Buoyancy is defined as the difference between the buoyancy force and the weight force, as the potential temperature, θ_v , as

The air of rising thermals is entrained from thermals possess positive

$$F|_{\zeta=0} = \frac{\partial F}{\partial z}|_{z=0} = 0, \quad F|_{\zeta=1} = 1, \quad \frac{\partial F}{\partial z}|_{\zeta=1} = G. \quad (8.2)$$

The evolution of the buoyancy profile (8.1) should satisfy the buoyancy transfer equation

$$\frac{\partial b}{\partial t} = -\frac{\partial B}{\partial z}, \quad (8.3)$$

where B is the vertical turbulent flux of buoyancy.

Integrating (8.3) over z from 0 to h_0 with due regard to the representation (8.1), and defining the top of the mixed layer as the buoyancy flux crossover height, i.e. taking $B=0$ at $z=h_0$, we obtain the mixed layer buoyancy budget equation

$$\frac{d}{dt} [N^2(h_0 + \Delta h) - \Delta b] = \frac{B_s}{h_0}, \quad (8.4)$$

where B_s is the near-surface value of the buoyancy flux.

Integration of (8.3) over z from 0 to $h_0 + \Delta h$ gives the equation of total buoyancy budget:

$$\frac{d}{dt} \left\{ \frac{1}{2} N^2(h_0 + \Delta h)^2 - \Delta b [h_0 + (1 - C_b)\Delta h] \right\} = B_s, \quad (8.5)$$

where $C_b(G) = \int_0^1 F(\zeta, G) d\zeta$ is the integral shape factor (Deardorff, 1979).

In accordance with (8.1) and (8.3), in the interfacial (entrainment) layer, at $h_0 \leq z \leq h_0 + \Delta h$, the buoyancy flux profile has the form

$$\begin{aligned} B = & \left[\int_0^\zeta F(\zeta', G) d\zeta' - G \frac{\partial}{\partial G} \int_0^\zeta F(\zeta', G) d\zeta' - \zeta \right] \frac{\Delta h}{h_0} B_s + \\ & + \left[F - G \int_0^\zeta F(\zeta', G) d\zeta' + G^2 \frac{\partial}{\partial G} \int_0^\zeta F(\zeta', G) d\zeta' \right] \Delta b \frac{dh_0}{dt} + \\ & + \left[\zeta F - (1 + G) \int_0^\zeta F(\zeta', G) d\zeta' - G(1 - G) \frac{\partial}{\partial G} \int_0^\zeta F(\zeta', G) d\zeta' \right] \Delta b \frac{d\Delta h}{dt}. \end{aligned} \quad (8.6)$$

Equations (8.4) and (8.5) are the two ordinary differential equations for three unknowns: h_0 , Δh and Δb . Additional relation is needed to close the problem. It can be derived from the consideration of the turbulent kinetic energy budget within the bulk of two adjacent layers, mixed layer and capping inversion layer.

For this purpose we may employ the balance equation for turbulent kinetic energy

$$\partial e / \partial t = B - \partial \Phi / \partial z - \varepsilon, \quad (8.7)$$

where e is the turbulent energy per unit of fluid mass, ε is its viscous dissipation rate, and Φ is the vertical flux of energy.

We adopt the hypothesis of similarity of convective regime considered, which states that the basic turbulence parameters, being normalized by the length scale $h_0 + \Delta h$ and the velocity scale $w_* = [B_s(h_0 + \Delta h)]^{1/3}$, cease to depend on time in their explicit form and depend on it only through these scales, i.e., they become universal functions of the dimensionless height $z/(h_0 + \Delta h)$. Hence, the vertical profiles of turbulent energy and its dissipation rate can be presented in the form

$$e = w_*^2 F_e \left(\frac{z}{h_0 + \Delta h} \right), \quad \varepsilon = \frac{w_*^3}{h_0 + \Delta h} F_\varepsilon \left(\frac{z}{h_0 + \Delta h} \right), \quad (8.8)$$

(8.2)

buoyancy transfer equation

(8.3)

representation (8.1), and height z ; i.e. taking $B=0$ at

(8.4)

of total buoyancy budget:

(8.5)

(1979).

(entrainment) layer, at

$\frac{h}{B_s} +$

$\frac{dh_0}{dt} +$

$B \frac{d\Delta h}{dt}$

(8.6)

itions for three unknowns: n. It can be derived from the bulk of two adjacent

ent kinetic energy

(8.7)

us dissipation rate, and Φ

nsidered, which states that h scale $h_0 + \Delta h$ and the

their explicit form and iversal functions of the turbulent energy and its

(8.8)

where F_e and F_ϵ are the universal functions satisfying boundary conditions $F_e(1)=F_\epsilon(1)=0$.

The employed closure hypothesis is similar to the one proposed by Deardorff (1970a,b), that has been widely used in so-called zero-order-jump models of the convective boundary layer, of which the most comprehensive was suggested by Zilitinkevich (1991). Instead of quite arbitrary height \bar{h} within the limits of the IL (usually close to the height of the buoyancy flux minimum), employed by these models, we use $h_0 + \Delta h$, i.e. the depth of the whole turbulized zone, as an appropriate length scale. The height \bar{h} is suitable for scaling the turbulence parameters in the major part of the convective boundary layer, but not within the IL (Zilitinkevich, 1991). In Section 8.2.3 (Figures 8.3 and 8.4) we shall see that utilisation of $h_0 + \Delta h$ allows to decrease the range of empirical estimates of the universal functions for e and ϵ precisely near the boundary layer top.

Termwise integration of (8.7) over z from 0 to $h_0 + \Delta h$ gives the following entrainment rate equation:

$$\begin{aligned} \frac{10}{3} C_e \left(1 + \frac{\Delta h}{h_0}\right)^{2/3} (E_h + E_\Delta) = & (1 - 2C_e) - 2C_e \frac{\Delta h}{h_0} - \left(1 - 2C_{bb} + 2G \frac{dC_{bb}}{dG}\right) \left(\frac{\Delta h}{h_0}\right)^2 + \\ & + 2 \left(C_b - GC_{bb} + G^2 \frac{dC_{bb}}{dG}\right) \frac{\Delta h}{h_0} Ri_b E_h + \\ & + 2 \left[C_b - 2C_{bb} - GC_{bb} - G(1-G) \frac{dC_{bb}}{dG}\right] \frac{\Delta h}{h_0} Ri_b E_\Delta - \\ & - \frac{4}{3} C_e \left(1 + \frac{\Delta h}{h_0}\right)^{5/3} De - 2 \frac{\Phi(h_0 + \Delta h)}{B_s h_0}, \end{aligned} \quad (8.9)$$

where $E_h = (B_s h_0)^{-1/3} dh_0 / dt$ is the dimensionless entrainment rate; $E_\Delta = (B_s h_0)^{-1/3} d\Delta h / dt$ is the dimensionless rate of changes of Δh ; $Ri_b = B_s^{-2/3} h_0^{1/3} \Delta b$ is the Richardson number based on the buoyancy increment across the IL; $De = B_s^{-4/3} h_0^{2/3} dB_s / dt$ is the non-stationarity parameter introduced in Deardorff et al. (1980) [following Zilitinkevich (1991) we call it the Deardorff number]; $C_e = \int_0^1 F_e(x) dx$ and $C_\epsilon = \int_0^1 F_\epsilon(x) dx$ are

dimensionless constants; $C_{bb} = \int_0^1 d\zeta \int_0^\zeta F(\zeta', G) d\zeta'$ is dimensionless function of G ;

$\Phi(h_0 + \Delta h)$ is the energy flux at the boundary layer top.

The energy drain from the boundary layer occurs due to the radiation of internal gravity waves into the stably stratified layer aloft. Thorpe (1973) expressed the maximum flux of energy for maintenance of propagating waves as $\Phi_{max} = (3\pi\sqrt{3})^{-1} N^3 A^2 \lambda$, where A and λ are the amplitude and the length of the waves respectively. In the framework of the simple bulk approach A and λ are usually determined from the similarity arguments. Kantha (1977) assumed A to be of the order of IL thickness, while λ is proportional to the mixed layer depth, h_0 . This yields

$$2 \frac{\Phi(h_0 + \Delta h)}{B_s h_0} = C_N Ri_N^{3/2} \left(\frac{\Delta h}{h_0}\right)^2, \quad (8.10)$$

where $Ri_N = B_s^{-2/3} h_0^{4/3} N^2$ is the Richardson number based on the buoyancy a frequency in the non-turbulent layer, C_N is a dimensionless constant.

Zilitinkevich (1991) argued that both A and λ are of the order of Δh , which gives

$$2 \frac{\Phi(h_0 + \Delta h)}{B_s h_0} = C_N' Ri_N^{3/2} \left(\frac{\Delta h}{h_0} \right)^3, \quad (8.11)$$

where C_N' is another dimensionless constant. There is still no clear experimental evidence of which expression of (8.10) and (8.11) is adequate (Fernando, 1991).

An approximation of the function $F(\zeta, G)$ fitting atmospheric and laboratory data reasonably well can be obtained from geometrical arguments. The simplest polynomial obeying the conditions (8.2) reads

$$F(\zeta, G) = \left(\frac{3}{2}G - 12 + 30C_b \right) \zeta^2 + (28 - 4G - 60C_b) \zeta^3 + \left(\frac{5}{2}G - 15 + 30C_b \right) \zeta^4. \quad (8.12)$$

The dimensionless constants C_e , C_ε , C_N or C_N' , and the shape factors $C_b(G)$ and $C_{bb}(G)$ in the above equations are to be determined from data of measurements (atmospheric and laboratory), and large-eddy simulations of convection.

In the following section the results of estimating the values of the above parameters from the empirical data, and the comparison of the calculated characteristics of the inversion layer with laboratory measurements will be presented.

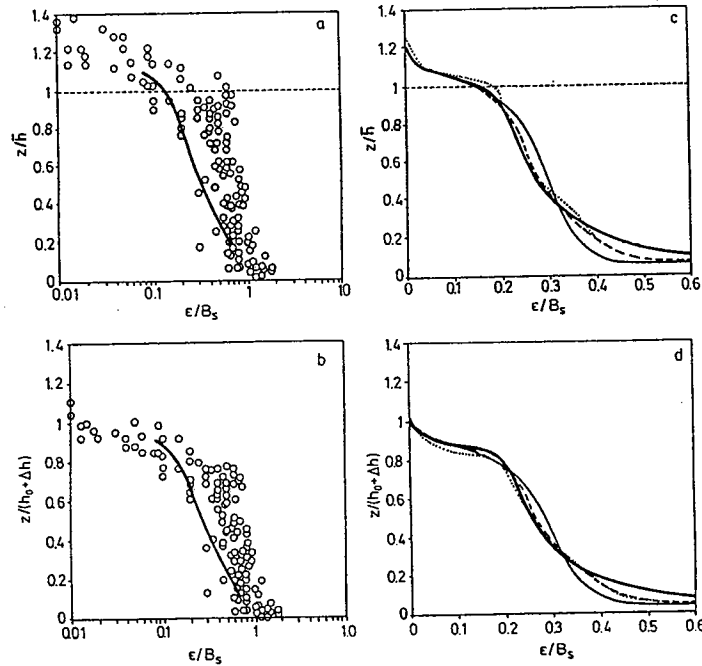


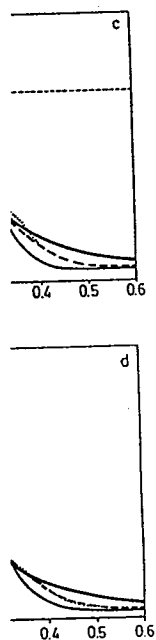
Figure 8.3. Empirical and LES data on dependence of dimensionless dissipation rate of turbulent kinetic energy, ε / B_s , on dimensionless height: (a), (c) - z/\bar{h} ; (b), (d) - $z/(h_0 + \Delta h)$. In (a) and (b) the points are the data from measurements in the atmosphere and the ocean (Caughy and Palmer, 1979; Lenschow et al., 1980; Shay and Gregg, 1986), the lines are from Deardorff and Willis (1985) laboratory experiments. In (c) and (d) the heavy solid lines show Mason's (1989) results, the solid lines are from Moeng's (1984) simulations; calculations by Nieuwstadt (1990), and Schmidt and Schumann (1989) are shown by dotted and dashed lines respectively. When the profiles of turbulent buoyancy flux were not given, the depth of the boundary layer, $h_0 + \Delta h$, was determined as the crossover height of the best fit curve.

(8.11)

experimental evidence of
).
eric and laboratory data
the simplest polynomial

$\left(5 + 30C_b\right) \zeta^4$. (8.12)

shape factors $C_b(G)$ and
measurements (atmospheric
the above parameters from
istics of the inversion layer



dimensionless dissipation rate of
a), (c) - z/\bar{h} ; (b), (d) -
ments in the atmosphere and
Shay and Gregg, 1986), the
its. In (c) and (d) the heavy
ure from Moeng's (1984)
and Schumann (1989) are
of turbulent buoyancy flux
determined as the crossover

8.2.3. Model parameters and calculation results. The constants C_e and C_e were evaluated by integrating the functions F_e and F_e obtained from measurements and large-eddy simulations (LES), over the whole turbulent zone. Summarizing the data from Figures 8.3-8.4 gave the values $C_e=0.3$ and $C_e=0.3$ as most appropriate for the shear-free case.

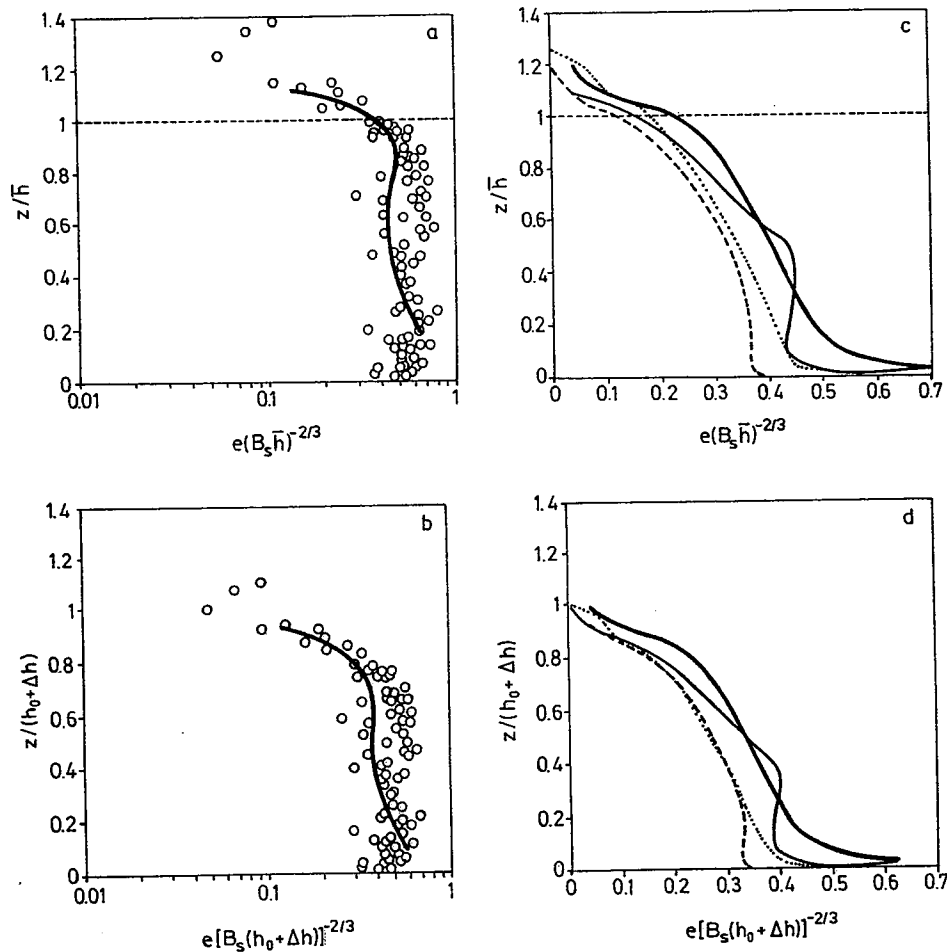


Figure 8.4. Vertical profiles of turbulent kinetic energy from measurements and LES: (a), (c) - the energy is scaled by $(B_s \bar{h})^{-2/3}$, the height is scaled by \bar{h} ; (b), (d) - the scales are $[B_s(h_0 + \Delta h)]^{-2/3}$ and $h_0 + \Delta h$, respectively. In (a) and (b) the points are the atmospheric data of Caughey and Palmer (1979), and Lenschow et al. (1980); the lines represent the laboratory measurements of Deardorff and Willis (1985). In (c) and (d) the LES results are shown. See Figure 8.3 for details.

We know of no direct measurements of the vertical energy flux at the IL top. Therefore, the only opportunity was to estimate dimensionless constants in (8.10) and (8.11) by comparing theoretical and empirical entrainment laws, i.e. the dependencies of the entrainment rate upon the Richardson numbers specified above. This was also a way to decide between the two expressions for wave-related vertical energy flux.

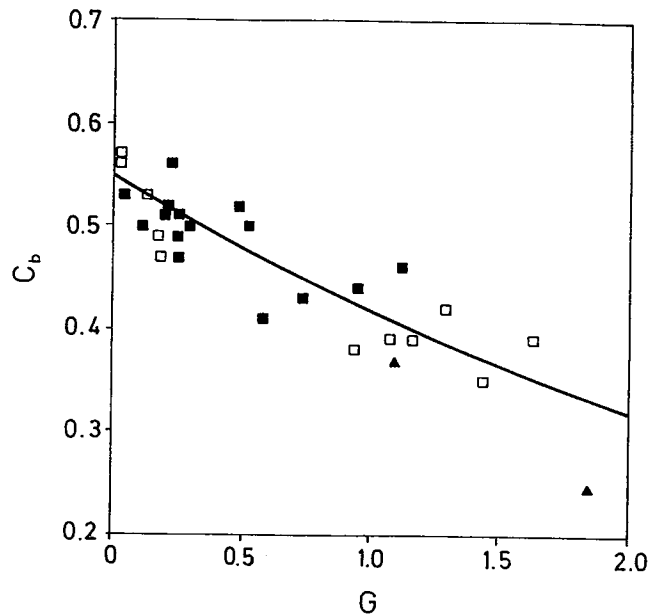


Figure 8.5. The integral shape factor C_b as function of relative stratification G . The open squares are laboratory data (Deardorff, 1979; Deardorff et al., 1980; Deardorff and Willis, 1985); the filled squares represent atmospheric data of Clarke et al. (1971), Chorley et al. (1975), Batchvarova and Gryning (1991); the triangles depict LES results of Mason (1989), and Schmidt and Schumann (1989). The line shows approximation (8.13).

Now we have to determine parameters of the function $F(\zeta, G)$. Figure 8.5 shows the dependence of C_b on G . The majority of C_b values lie between 0.35 and 0.55. The maximum value corresponding to the two-layer fluid system is 0.57. Within the observed range of G variations exponential function proposed by Deardorff (1979)

$$C_b = 0.55 \exp(-0.27G) \quad (8.13)$$

fits the empirical data fairly well.

According to (8.12), function $C_{bb}(G)$ in equation (8.9) is

$$C_{bb} = \frac{1}{120}G - \frac{1}{10} + \frac{1}{2}C_b. \quad (8.14)$$

The empirical dependence of C_{bb} on G is shown in Figure 8.6 together with the curve calculated from equations (8.13) and (8.14). The scatter of points about the curves in Figures 8.5 and 8.6 is rather small despite the different sources of the data. This justifies the use of a simple polynomial profile (8.12), at least as a first approximation.

The model developed assumes that mean velocity shear has only a minor contribution to the total energy budget. Very few atmospheric data match this assumption. Shear-free penetrative convection was thoroughly studied in the series of laboratory experiments by Deardorff et al. (1969; 1980; Willis and Deardorff, 1974; Deardorff and Willis, 1985). The most comprehensive data set was presented in Deardorff et al. (1980, hereafter referred to as DWS). It was used to test the model.

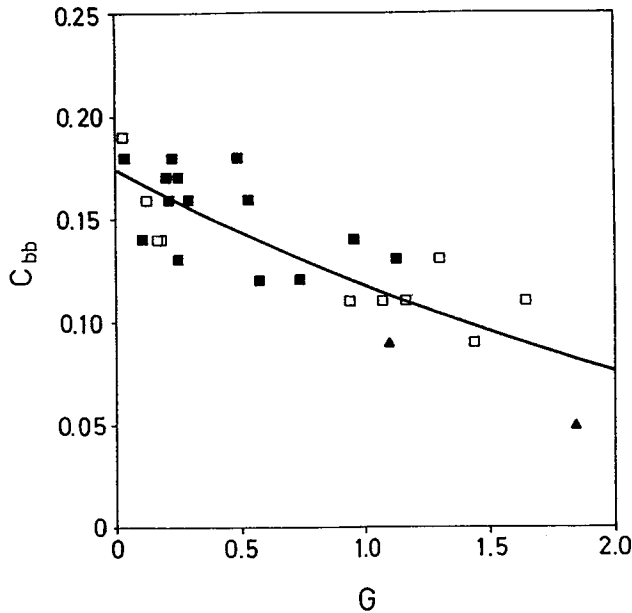
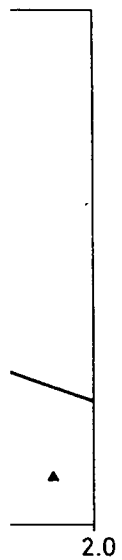


Figure 8.6. The dependence of dimensionless parameter C_{bb} on relative stratification G . Markers are the same as in Figure 8.5. The curve is drawn after equations (8.13) and (8.14).

The results of laboratory experiments and model simulations can be conveniently represented in the form of an entrainment law. A traditional way originating from the zero-order-jump approach is to express the entrainment rate and Richardson numbers in terms of \bar{h} , as follows:

$$\bar{E} = (B_s \bar{h})^{-1/3} d\bar{h} / dt, \quad \bar{Ri}_b = B_s^{-2/3} \bar{h}^{1/3} \Delta b, \quad \bar{Ri}_N = \frac{1}{2} B_s^{-2/3} \bar{h}^{4/3} N^2. \quad (8.15)$$

Our model allows to determine \bar{h} directly from the shape of the buoyancy flux profile (8.6) as the height of the buoyancy flux minimum.

The entrainment relation for a two-layered fluid ($\bar{Ri}_N=0$) calculated by the model is depicted in Figure 8.7. It was obtained from the solution of system (8.4), (8.5), (8.9). Variations of the bottom buoyancy flux with time were neglected in the entrainment equation, as they are not important in most interesting cases including the DWS experiments (see Zilitinkevich, 1991). The initial conditions for h_0 and Δb define the initial Richardson number Ri_b . Depending upon the initial Δh value, dimensionless entrainment rate does not reveal unique dependence on Richardson number at the early stage of the buoyancy profile evolution when non-stationarity of the entrainment zone plays an important part. However, as time passes, the curves corresponding to different initial $\Delta h/h_0$ converge to a unique curve showing a quasi-equilibrium entrainment regime. The initial period of adjustment is not illustrated in Figure 8.7.

stratification G . The open squares; Deardorff and Willis, et al. (1971), Chorley et al. (1971), Mason (1989), and (8.13).

Figure 8.5 shows the curves between 0.35 and 0.55. The results of Mason (1989), and (8.13).

(8.13)

(8.14)

together with the curve about the curves in Figures. This justifies the use of a

only a minor contribution to the assumption. Shear-free laboratory experiments by Deardorff and Willis, 1985). The results of Mason (1989), hereafter referred to as

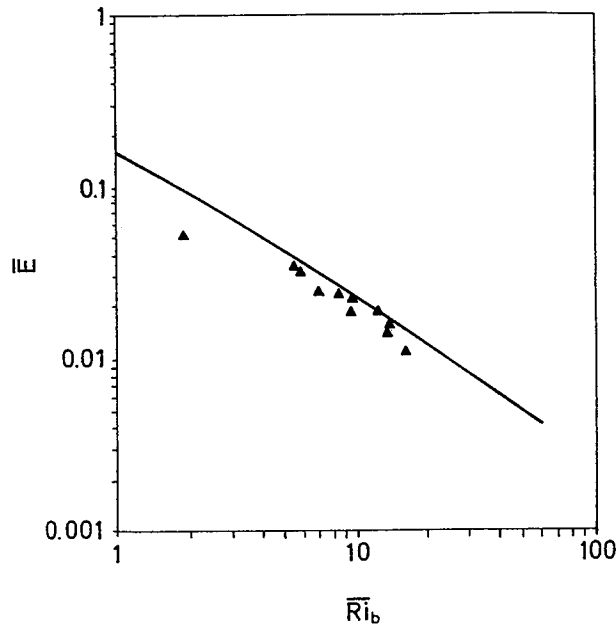


Figure 8.7. Dimensionless entrainment rate \bar{E} versus Richardson number \bar{Ri}_b for a two-layer fluid system. The model curve is shown by the solid line; the points are from the Deardorff et al. (1980) laboratory experiments.

In the quasi-equilibrium entrainment regime model predictions agree well with the data from two-layer fluid experiments of DWS. The dependence of \bar{E} versus \bar{Ri}_b , shown in Figure 8.7, practically coincides with the basic relation of the zero-order model, $\bar{E} \cdot \bar{Ri}_b = \text{const.}$

Figure 8.8 displays $\Delta h/h_0$ as function of \bar{Ri}_b in the two-layer fluid system. As seen from the plot, the model predicts $\Delta h/h_0$ to increase with increasing \bar{Ri}_b , while the DWS data show weak inverse dependence. This fact cannot be explained by the zero-order model that predicts $\Delta h/h_0$ to increase linearly at small \bar{Ri}_b approaching constant at $\bar{Ri}_b \gg 1$. Our model results suggest that the DWS experiments inclined to study the two-layer fluid system were performed on the background of weak stable density stratification in the quiescent layer. The data from Table 1 of DWS indicate that stable lapse rate was always present at the IL top, even in experiments aimed to simulate two-layer fluid. The $\Delta h/h_0$ values from these experiments are plotted against \bar{Ri}_b in Figure 8.9 with due regard to non-zero values of N^2 . They conform fairly well with the theoretical curve for a linearly stratified fluid at small \bar{Ri}_b .

The model developed is able to reproduce the hysteresis-type relationships between the entrainment parameters, resulting from the convective boundary layer development through consecutive transition stages in a multi-layer fluid. The hysteresis entrainment zone behaviour was observed in the day-time atmospheric boundary layer (Nelson et al., 1989). This effect is qualitatively illustrated in Figure 8.10 showing the results of simulation of entrainment in a three-layer system: neutral lower layer - linearly stratified layer - neutral upper layer. The normalized IL depth grows with time during the transition period of the convective boundary layer development, whereas the Richardson number diminishes. The present model is suitable to simulate such a behaviour when the effects of wind-shear and large-scale subsidence are weak.

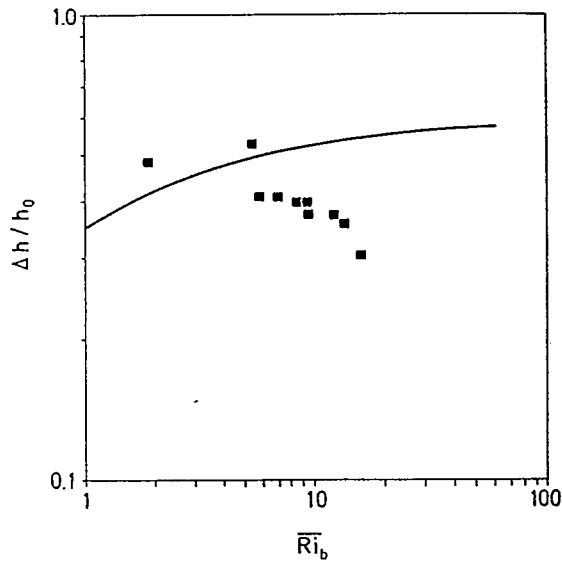


Figure 8.8. Normalized entrainment layer depth $\Delta h / h_0$ versus \overline{Ri}_b in a two-layered fluid. The curve is calculated by the present model; the points are from the Deardorff et al. (1980) laboratory experiments.

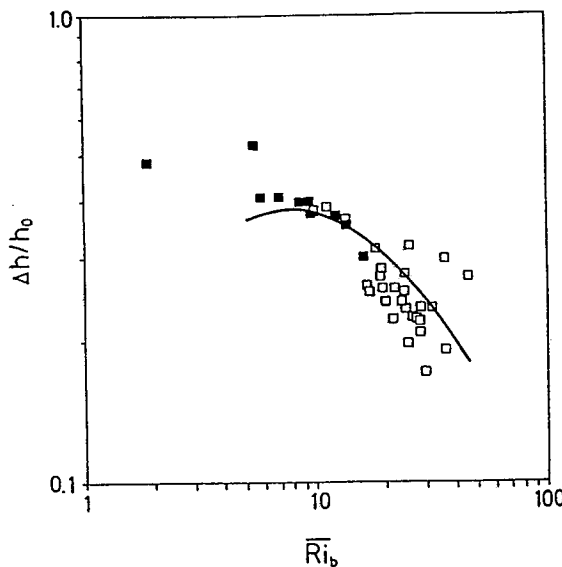


Figure 8.9. Normalized entrainment layer depth $\Delta h / h_0$ versus \overline{Ri}_b in a linearly stratified fluid. The curve is calculated by the present model, employing formula (8.11) with $C_N' = 0.012$ to parameterize the wave-related energy drain; the open squares represent the DWS data referring to a linearly stratified fluid. The DWS data from the experiments intended to treat a two-layer fluid system are also shown (filled squares).

on number \overline{Ri}_b for a two-
; the points are from the
s agree well with the data
 \overline{E} versus \overline{Ri}_b , shown in
f the zero-order model,

fluid system. As seen from
 \overline{Ri}_b , while the DWS data
the zero-order model that
ant at $\overline{Ri}_b \gg 1$. Our model
o-layer fluid system were
in the quiescent layer. The
ays present at the IL top,
 $\Delta h / h_0$ values from these
to non-zero values of N^2 .
ratified fluid at small \overline{Ri}_b .

relationships between the
ayer development through
teresis entrainment zone
ayer (Nelson et al., 1989).
ie results of simulation of
ly stratified layer - neutral
he transition period of the
n number diminishes. The
fects of wind-shear and

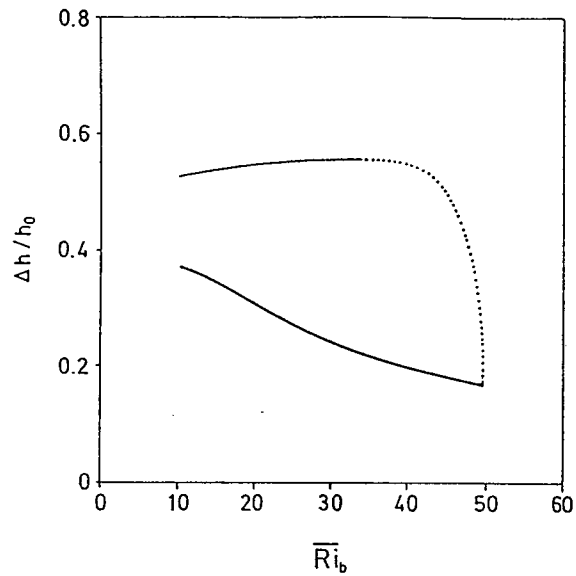


Figure 8.10. Convective boundary layer development in a three-layered fluid. The heavy solid curve corresponds to the entrainment in a linearly stratified layer. The dotted curve represents the transition period of the boundary layer development when $\Delta h / h_0$ adjusts to a regime characteristic of a two-layer system. The solid line displays quasi-equilibrium entrainment in a two-layered fluid.

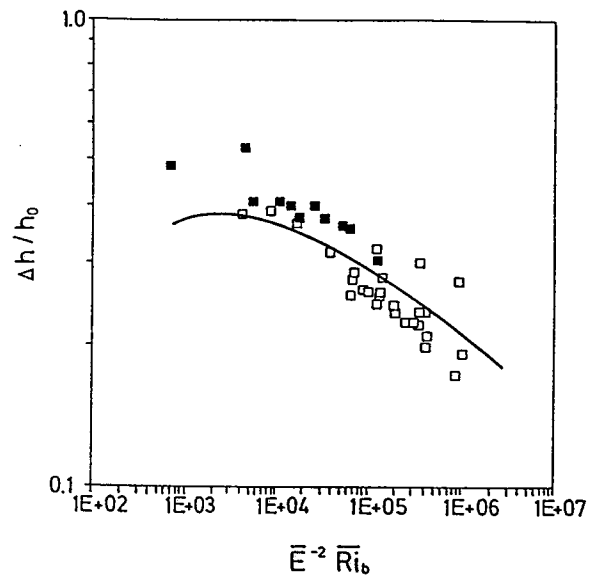


Figure 8.11. Normalized entrainment layer depth $\Delta h / h_0$ versus dimensionless combination $\bar{E}^{-2} \cdot \bar{Ri}_b$ in a linearly stratified fluid. The curve is calculated by the present model; the markers are the same as in Figure 8.9.

It is worth mentioning that the spread of data about the theoretical curve in Figure 8.9 is rather large. Basic equations of the model (8.4), (8.5) and (8.9) indicate that normalized entrainment layer depth is the function of several dimensionless parameters (dimensionless entrainment rate, Richardson numbers, the rate of changes of the IL thickness). Therefore, one can hardly expect empirical data to order well if $\Delta h/h_0$ is presented as a function of the only parameter (\overline{Ri}_b in Figure 8.9). Gryning and Batchvarova (1993, personal communication) processed the data on $\Delta h/h_0$ in terms of combination $Ri_E = \overline{E}^{-2} \overline{Ri}_b$, which they called the entrainment Richardson number. This reduced the scatter of empirical points on the graph $\Delta h/h_0$ versus Ri_E as compared to $\Delta h/h_0$ versus \overline{Ri}_b . As follows from the above analysis, h_0 may be strongly affected by the non-stationarity of the boundary layer. This effect is not explicitly incorporated by empirical dependence of $\Delta h/h_0$ on \overline{Ri}_b . The data from the DWS experiments processed in terms of $\overline{E}^{-2} \overline{Ri}_b$ are shown in Figure 8.11. Taking explicit account of \overline{E} aligns the DWS data with the theoretical predictions of the present model.

8.3. Stable boundary layer

8.3.1. Characteristics and structure. Within the stable boundary layer the greatest static stability is near the ground. It decreases smoothly towards neutral with height (Figure 8.12). In reality not the whole SBL can be classified as the inversion layer for the inverse temperature gradients can be observed usually only in the lower portion of it. Nevertheless the entire SBL is loosely called the inversion layer or nocturnal inversion (Stull, 1988).

The wind speed in the SBL increases with height, reaching maximum close to the top of the stable layer (Figure 8.12). In this maximum the wind speed is supergeostrophic in some cases. The layer with supergeostrophic wind speed values is called the nocturnal jet. Above the jet, the wind speed and direction smoothly change to geostrophic. Beneath the jet wind direction strongly veer with height. A variety of physical mechanisms can cause the formation of the nocturnal jet. The two main of them are baroclinicity over sloping terrain, and the inertial oscillation.

The angle between the wind direction and isobars in SBL is typically rather large close to the surface and changes rapidly in the vertical as wind approaches the geostrophic value.

While turbulent motions are suppressed by stability in SBL, the buoyancy (gravity) waves can be generated and spread in the statically stable environment. Turbulence can non-linearly interact with the waves. It is not very easy to distinguish between turbulence and strongly non-linear waves in the SBL flows.

From the point of view of turbulence intensity stable boundary layers can range from being well mixed to non-turbulent. With stable stratification the buoyancy forces are damping the turbulence, making it sporadic and patchy, what may lead to the decoupling of the boundary layer from surface forcings. Since there is very little vertical mixing in SBL, temperature, humidity, and turbulence can display the fine-scale vertical structure within this layer.

Wind shears are virtually the only sources of turbulence in the SBL. Turbulence, when averaged over long times, decreases smoothly towards the top of the SBL. In some situations, turbulence is continuous over the whole depth of the layer; in other cases it might be patchy, weak and intermittent, so that only being time averaged over a couple of hours the resulting turbulence flux might appear to be acting over the whole SBL depth.

For such continuous and contiguous turbulence cases, surface forcings can be used as the key scaling parameters for the SBL structure (Stull, 1988). In this situation stably stratified turbulent flow is assumed to be in equilibrium with the surface, and similarity theory considerations are applied to construct the models. A theory of the above type was proposed by Zilitinkevich (1989a,b). It is shown in the next section how it can be used as a basis for the calculation of the dynamic and thermal structure of the stable boundary layer.

60

2-layered fluid. The heavy
d layer. The dotted curve
when $\Delta h/h_0$ adjusts to a
splays quasi-equilibrium

1E+07

z_0 versus dimensionless
calculated by the present

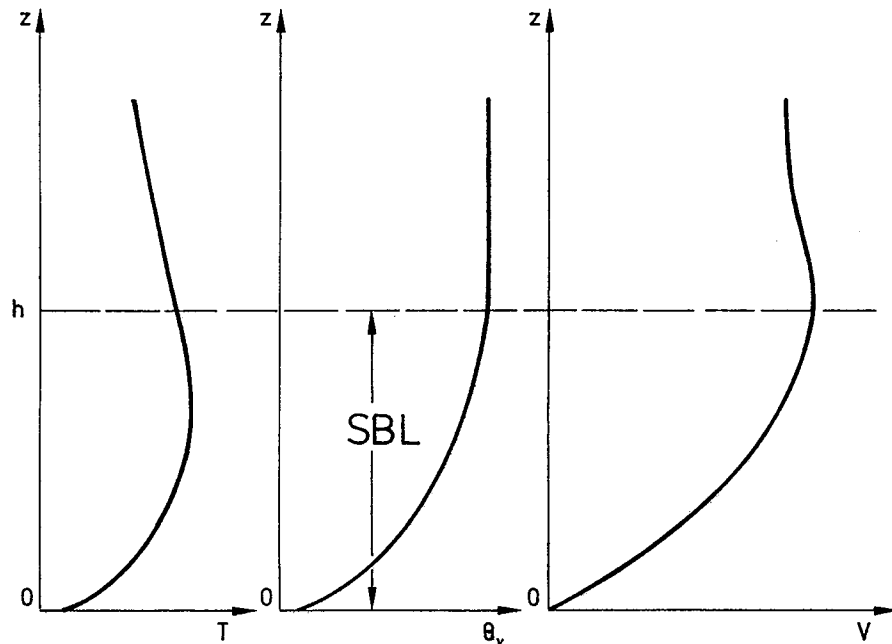


Figure 8.12. Profiles of wind speed and temperature in an idealized stable boundary layer. After Stull (1988).

8.3.2. Parameterization of wind and temperature profiles in SBL. It may be assumed that in continuously/contiguously turbulent SBL the structure of the layer at each moment of time is determined by the parameters characterizing the instantaneous situation. In case the source of buoyant forcing is located at the ground, its effect can be characterized by the near-surface value of the vertical buoyancy flux, B_s , or by the two other parameters related to it, the Monin-Obukhov length scale $L = -u_*^3 / (kB_s)$ and the non-dimensional stratification parameter $\mu = -k^2 B_s / (|f|u_*^2)$, where k is the von Karman constant (we shall use its mostly accepted value $k=0.4$), f is the Coriolis parameter, and u_* is the friction velocity.

At neutral stratification ($B_s=0$) buoyant forces do not act, at stable stratification ($B_s<0$) they suppress turbulence.

With the neutral stratification, the boundary layer depth is expressed by the Rossby-Montgomery formula: $h = \Lambda_0 u_* / |f|$, where Λ_0 is a non-dimensional universal constant which value can be adopted equal 0.3 (Zilitinkevich, 1989a).

With the stable stratification, the case we are interested in, the list of governing parameters determining the boundary-layer depth should be supplemented by some additional parameter related to the surface buoyancy flux.

In the case of sufficiently strong stability, when $\mu \gg 1$, boundary layer depth can be expressed as (Zilitinkevich, 1972):

$$h = C_h u_*^2 |f B_s|^{-1/2}, \quad (8.16)$$

where C_h is a non-dimensional universal constant of the order of unity.

The simplest interpolation formula combining Rossby-Montgomery expression and (8.16) has the form [Zilitinkevich (1989a)]:

$$\frac{|f|h}{u_*} = \Lambda(\mu) = \left(\frac{1}{\Lambda_0} + \frac{\mu^{1/2}}{kC_g} \right)^{-1} \quad (8.17)$$

When SBL is stationary and horizontally homogeneous, the velocity components u and v along the corresponding horizontal axes x and y satisfy the Ekman equations

$$f(v - U_g \sin \alpha) + \frac{d\tau_x}{dz} = 0, \quad -f(u - U_g \cos \alpha) + \frac{d\tau_y}{dz} = 0, \quad (8.18)$$

where z is height, $U_g \cos \alpha$ and $U_g \sin \alpha$ are components of the geostrophic wind vector (U_g is modulus of this vector, α is the angle between it and the x -axis), τ_x and τ_y are the components of the vertical turbulent flux of momentum, normalized by density. Let us direct the x -axis along the surface friction vector. The surface friction will be characterized then by the wind turn angle α and the friction velocity $u_* = \sqrt{\tau_{xs}}$. At the upper boundary of SBL, at $z=h$, the turbulence degenerates, so the vertical turbulent momentum flux reduces to zero:

$$\tau_x(h) = \tau_y(h) = 0, \quad (8.19)$$

and the wind becomes geostrophic:

$$u(h) = U_g \cos \alpha, \quad v(h) = U_g \sin \alpha. \quad (8.20)$$

Integrating equations (8.18) over z from 0 to h , taking into account the boundary conditions (8.19) and (8.20), we obtain

$$\int_0^h u dz = hu(h), \quad \int_0^h v dz = hv(h) + u_*^2 / f. \quad (8.21)$$

The SBL velocity profile at $z \ll h$, $z \ll L$ satisfies the near-surface logarithmic law:

$$u(z) = \frac{u_*}{k} \ln \frac{z}{z_0}, \quad v(z) = 0, \quad (8.22)$$

where z_0 is the roughness parameter, and the velocity defect law at $z \gg z_0$:

$$U_g \cos \alpha - u(z) = \frac{u_*}{k} \phi_u(\zeta, \mu), \quad U_g \sin \alpha - v(z) = -\frac{u_*}{k} \phi_v(\zeta, \mu) \text{sign} f, \quad (8.23)$$

where ζ is a non-dimensional height $\zeta = z/h$, and $\phi_u(\zeta, \mu)$, $\phi_v(\zeta, \mu)$ are universal functions which have to satisfy, in accordance with (8.20), the conditions $\phi_u(1, \mu) = \phi_v(1, \mu) = 0$.

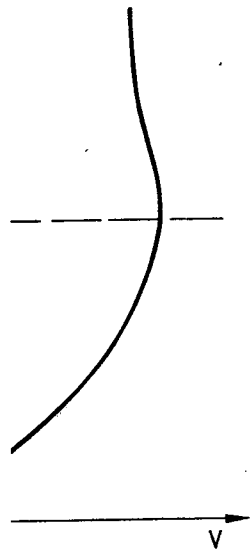
Overlapping of formulas (8.22) and (8.23) in the region $z_0 \ll z \ll h$, where both hold true, gives the resistance law

$$\ln(C_g Ro) - B(\mu) = \sqrt{\left(\frac{k}{C_g} \right)^2 - A^2(\mu)}, \quad \sin \alpha = \frac{-A(\mu)}{k} C_g \text{sign} f, \quad (8.24)$$

where $Ro = U_g / (|f|z_0)$ is the surface Rossby number, $C_g = u_* / U_g$ is the geostrophic drag coefficient, $A(\mu)$ and $B(\mu)$ are non-dimensional functions of μ .

According to (8.17), (8.22-8.24) the velocity profile in the SBL can be represented as

$$u(z) = \frac{u_*}{k} \left[\ln \frac{z}{z_0} + f_u(\zeta, \mu) \right], \quad v(z) = -\frac{u_*}{k} f_v(\zeta, \mu) \text{sign} f, \quad (8.25)$$



ed stable boundary layer.

les in SBL. It may be
cture of the layer at each
instantaneous situation. In
t can be characterized by
he two other parameters
and the non-dimensional
rman constant (we shall
r, and u_* is the friction

able stratification ($B_s < 0$)

h is expressed by the
n-dimensional universal
a).

it of governing parameters
ome additional parameter

ndary layer depth can be

$$(8.16)$$

nity.

ery expression and (8.16)

where $f_u(\zeta, \mu) = -B(\mu) - \ln[\Lambda(\mu)\zeta] - \phi_u(\zeta, \mu)$ and $f_v(\zeta, \mu) = A(\mu) - \phi_v(\zeta, \mu)$ are functions of two dimensionless arguments, satisfying the conditions

$$f_u(0, \mu) = f_v(0, \mu) = 0, \quad (8.26)$$

$$f_u(1, \mu) = -B(\mu) - \ln \Lambda(\mu), \quad f_v(1, \mu) = A(\mu). \quad (8.27)$$

With due regard to these conditions we can approximate functions f_u and f_v by the following quadratic polynomials:

$$f_u(\zeta, \mu) = b(\mu)\zeta + b^*(\mu)\zeta^2, \quad f_v(\zeta, \mu) = a(\mu)\zeta + a^*(\mu)\zeta^2, \quad (8.28)$$

whose coefficients $a(\mu)$, $a^*(\mu)$, $b(\mu)$, $b^*(\mu)$, according to (8.21), are connected in pairs

$$b^*(\mu) = -\frac{3}{2} - \frac{3}{4}b(\mu), \quad a^*(\mu) = \frac{3k}{2\Lambda(\mu)} - \frac{3}{4}a(\mu). \quad (8.29)$$

The function $\Lambda(\mu)$ is known from (8.17). To find $a(\mu)$ and $b(\mu)$ we shall use one of the results of the Monin-Obukhov similarity theory for the surface layer, namely the logarithmic + linear law for the velocity profile at $z \ll h$ and $L \ll h$:

$$u(z) = \frac{u_*}{k} \left(\ln \frac{z}{z_0} + \beta_u \frac{z}{L} \right), \quad v(z) = 0, \quad (8.30)$$

where β_u is a non-dimensional constant, which value is about 5 (Dyer, 1974). Matching approximation (8.25) with the near-surface formulation (8.30) we are coming to

$$b(\mu) = b_0 + C_h \beta_u \mu^{1/2}, \quad a(\mu) = a_0, \quad (8.31)$$

where a_0 and b_0 can be expressed through A_0 and B_0 , which are the analogs of $A(\mu)$ and $B(\mu)$ for the neutral case (Zilitinkevich, 1989a):

$$b_0 = 6 - 4B_0 - 4\Lambda_0, \quad a_0 = 4A_0 - 6k / \Lambda_0, \quad (8.32)$$

Values of universal constants A_0 , B_0 and C_h were determined by Zilitinkevich from the data of laboratory and atmospheric measurements: $A_0 = 4.5$, $B_0 = 1.7$, and $C_h = 0.85$.

By substituting the resulting expressions of f_u and f_v into relations (8.27) the explicit formulas for $A(\mu)$ and $B(\mu)$ can be obtained:

$$A(\mu) = A_0 + \frac{3}{2C_h} \mu^{1/2}, \quad B(\mu) = B_0 + \ln \left(1 + \frac{\Lambda_0 \mu^{1/2}}{kC_h} \right) - \frac{1}{4} C_h \beta_u \mu^{1/2}. \quad (8.33)$$

The above expressions completely specify the resistance law for the SBL provided the constants k , Λ_0 , A_0 , B_0 , C_h , β_u , and the values of f , U_g , B_s , and z_0 are known.

From the same considerations the expression for the temperature profile in SBL is derived. According to Zilitinkevich's (1975) similarity theory, in quasi-stationary SBL the temperature defect law holds

$$\theta_h - \theta(z) = \frac{\theta_*}{k} \phi_\theta(\zeta, \mu), \quad (8.34)$$

as well as the heat transfer law

$u) - \phi_v(\zeta, \mu)$ are functions

(8.26)

(8.27)

actions f_u and f_v by the

$\mu)^{\zeta^2}$, (8.28)

l), are connected in pairs

(8.29)

u) we shall use one of the surface layer, namely the

(8.30)

5 (Dyer, 1974). Matching are coming to

(8.31)

the analogs of $A(\mu)$ and

(8.32)

and by Zilitinkevich from the 1.7, and $C_h=0.85$.

relations (8.27) the explicit

$C_h \beta_u \mu^{1/2}$. (8.33)

for the SBL provided the and z_0 are known.

perature profile in SBL is in quasi-stationary SBL the

(8.34)

$$(\theta_h - \theta_s) / \theta_s = \frac{1}{k} \ln(u_s / fz_{0T}) - C(\mu), \quad (8.35)$$

where z_{0T} is the roughness parameter with respect to temperature, θ is the potential temperature, θ_h and θ_s are its values at the SBL upper boundary and at the underlying surface, respectively, θ_s is the temperature scale, $C(\mu)$ is the universal function of μ , and ϕ_θ is the universal function of ζ and μ .

Overlapping the above two formulas and employing the representation (8.17) for the SBL depth, we obtain the following expression for the potential temperature profile in quasi-stationary SBL:

$$\theta(z) = \theta_s + \frac{\theta_s}{k} \left[\ln \frac{z}{z_{0T}} + f_\theta(\zeta, \mu) \right], \quad (8.36)$$

where $f_\theta = -C(\mu) - \ln[\Lambda(\mu)\zeta] - \phi_\theta$ is a universal function of ζ and μ , satisfying the conditions:

$$f_\theta(0, \mu) = 0, \quad f_\theta(1, \mu) = -C(\mu) - \ln \Lambda(\mu). \quad (8.37)$$

These conditions allow us to represent function $f_\theta(\zeta, \mu)$ in the form of a square polynomial

$$f_\theta(\zeta, \mu) = c(\mu)\zeta + c^*(\mu)\zeta^2, \quad (8.38)$$

in which coefficients $c(\mu)$ and $c^*(\mu)$ are universal functions of μ .

Taking the first of conditions (8.37) and assuming that at the top of SBL the vertical gradient of potential temperature tends to zero, we have $c^*(\mu) = -1/2c(\mu) - 1/2$. Employing the Monin-Obukhov's logarithmic + linear law for temperature profile in the surface layer we can obtain the expression relating $c(\mu)$ to $C(\mu)$ and $\Lambda(\mu)$: $c(\mu) = 1 - 2C(\mu) - 2 \ln \Lambda(\mu)$, which finally yields the representation of the function $C(\mu)$:

$$C(\mu) = C_0 + \ln \left(1 + \frac{\Lambda_0 \mu^{1/2}}{k C_h} \right) - \frac{1}{2} C_h \beta_\theta \mu^{1/2}, \quad (8.39)$$

in which the recommended value of C_0 is 3.7 (Zilitinkevich, 1989a), and β_θ can be taken equal to β_u (Dyer, 1974).

In the dry-atmosphere case the expression (8.36) provides for the opportunity to replace the surface buoyancy flux in the list of external parameters by the difference of temperatures at two given layers within the SBL.

The heat transfer law combined with the resistance law gives the convenient formulation for calculating the dynamic and thermal structure of the SBL in terms of external parameters, such as geostrophic wind velocity and temperature difference across the layer.

8.3.3. Calculation procedure and examples of calculated profiles. The list of external parameters for calculating wind and temperature profiles in SBL includes:

geographic latitude of the point in which the profiles are calculated φ ;

modulus of the geostrophic wind velocity U_g ;

roughness parameter z_0 ;

air temperature at the first (lower) level T_1 ;

air temperature at the second (upper) level T_2 .

The Coriolis parameter is related to latitude by the well known formula: $f = 2\omega \sin \varphi$, where ω is the angular velocity of the earth. The potential temperature values at the reference

levels (θ_1 and θ_2 respectively) can be obtained from T_1 and T_2 provided the elevations of the levels and reference pressure (often it is possible to prescribe $p_0=1000\text{hPa}$) are known.

If the potential temperature difference between the reference layers is very small, the layer should be considered as a neutral one. There is no buoyant forcing with the neutral stratification, and therefore $\mu = B_s = 0$. The wind profile in this case is obtained from the system of equations (8.17), (8.25), (8.28), (8.29), (8.32), supplemented by the expressions

$$u_* = U_g k \left\{ \left[\ln(h/z_0) - B_0 - \ln \Lambda_0 \right]^2 + A_0^2 \right\}^{-1/2}, \quad (8.40)$$

$$\alpha = -\arcsin \left(\frac{A_0 u_*}{k U_g} \right), \quad (8.41)$$

derived by combining (8.24) and (8.25) at $z=h$, taking into account that with neutral stratification $\mu=0$.

With stable stratification, when $\theta_2 > \theta_1$, the temperature increment $\Delta\theta = \theta_2 - \theta_1$ can be employed for calculating the temperature scale θ_s , by excluding θ_s , and z_{0T} from (8.36):

$$\theta_s = \Delta\theta k \left[\ln(z_2/z_1) + c(\mu)(z_2 - z_1)/h + c^*(\mu)(z_2^2 - z_1^2)/h^2 \right]^{-1}, \quad (8.42)$$

and evaluating the stratification parameter μ which can be expressed through θ_s and u_* as:

$$\mu = k^2 \beta \theta_s / (f u_*), \quad (8.43)$$

where $\beta = g/\bar{\theta}$ is the buoyancy parameter, and $\bar{\theta}$ is the reference value of the potential temperature.

To calculate the temperature profile using formula (8.36) we need additional equation for roughness length with regard to temperature z_{0T} . One of the possible ways to relate z_{0T} to z_0 was suggested by Brutsaert (1982):

$$z_{0T} = 7.4 z_0 \exp \left[-2.46 \left(\frac{u_* z_0}{\nu} \right)^{0.25} \right], \quad (8.44)$$

where ν is the kinematic viscosity of the air. In combination with equation (8.36) applied to each reference level for temperature, Brutsaert's formula provides the values of three parameters: θ_s , z_{0T} and θ_s [see (8.42)]. The surface temperature value is presented by the formula following from (8.36):

$$\theta_s = \theta_i - \frac{\theta_s}{k} \left[\ln \frac{z_i}{z_{0T}} + f_\theta(\zeta_i, \mu) \right], \quad (8.45)$$

where i is the number of any of the reference levels for temperature, and $\zeta_i = z_i/h$.

Together with equations (8.17), (8.25), (8.28), (8.29), (8.32), (8.36), (8.38), (8.39) and expressions for surface friction parameters u_* and α [they are derived easily from (8.24) and (8.25) in the same way as equations (8.40) and (8.41)]:

$$u_* = U_g k \left\{ \left[\ln(h/z_0) - B(\mu) - \ln \Lambda(\mu) \right]^2 + A(\mu)^2 \right\}^{-1/2}, \quad (8.46)$$

$$\alpha = -\arcsin \left[\frac{A(\mu) u_*}{k U_g} \right] \quad (8.47)$$

expressions (8.42)-(8.45) constitute the system for calculating the velocity and temperature profiles in the stable boundary layer.

Both systems presented above include non-linear equations. To solve them by any of iterative methods, it is necessary to prescribe the initial values of one or several parameters to

ided the elevations of the (00hPa) are known. rs is very small, the layer forcing with the neutral ase is obtained from the ented by the expressions

$$(8.40)$$

$$(8.41)$$

ccount that with neutral ment $\Delta\theta = \theta_2 - \theta_1$ can be and z_{0T} from (8.36):

$$h^2]^{-1}, \quad (8.42)$$

d through θ_s and u_s as:

$$(8.43)$$

ice value of the potential ed additional equation for ble ways to relate z_{0T} to

$$(8.44)$$

equation (8.36) applied to vides the values of three : value is presented by the

$$(8.45)$$

$\zeta_i = z_i / h$. (8.36), (8.38), (8.39) and rived easily from (8.24)

$$(8.46)$$

$$(8.47)$$

e velocity and temperature

To solve them by any of one or several parameters to

be determined. In the case of neutral stratification, the value of the friction velocity can be prescribed, for example as a fraction of U_g . With stable stratification, it is convenient to define also the initial value of θ_s , taking the logarithmic law as the first approximation for the temperature profile. Starting with these two parameters we can calculate the initial values of h and μ , employing formulas (8.17) and (8.43), respectively. Substitution of μ into equations (8.17), (8.29), (8.31), (8.33), and (8.39) gives the values of μ -dependent functions and coefficients of the polynomials in the representations of the velocity and temperature profiles. This allows to calculate the new approximations for the temperature scale and the friction velocity, using equations (8.42) and (8.46). The above cycle is repeated till the convergence is achieved. After that the profiles and their supplementary parameters (α , θ_s , z_{0T}) can be calculated from the equations (8.25), (8.28), (8.36), (8.38), (8.44), (8.45), and (8.47).

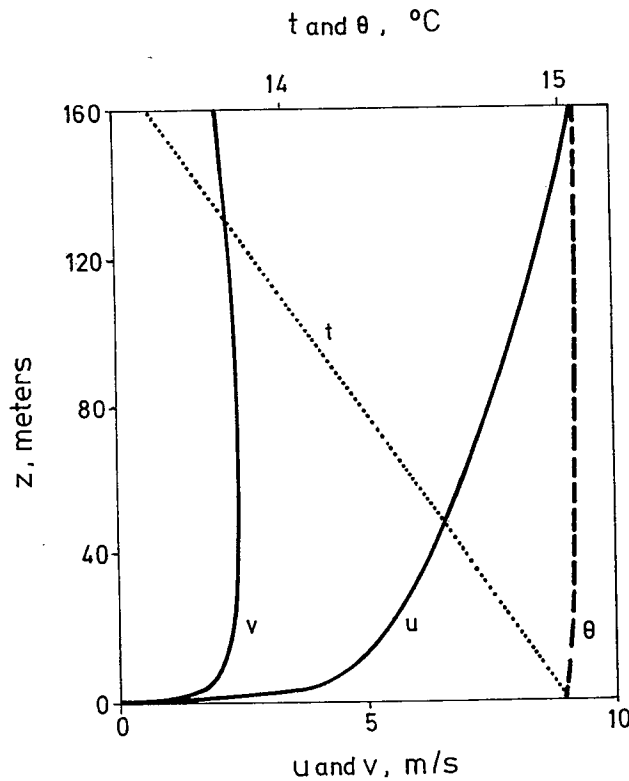


Figure 8.13. Simulated profiles of wind speed and temperature in the stable boundary layer under the conditions of very weak stratification.

The presented formulations and calculation procedure were used for simulation of the vertical structure of SBL with different rates of stability.

The examples of the calculated profiles for the boundary layer with very weak stratification, i.e., for the nearly neutral case, when μ is close to zero, are presented in Figure 8.13. The following values of the external parameters were prescribed for this case: $\varphi=45^\circ$; $U_g=10\text{m/s}$; $z_0=5\text{cm}$; $T_1=15^\circ\text{C}$ ($z_1=0.5\text{m}$); $T_2=15^\circ\text{C}$ ($z_2=2.0\text{m}$). The resulting velocity vector was rotated by the calculated angle α to transfer velocity components into the co-ordinate system with x -axis parallel to the geostrophic wind. The temperature profile in Figure 8.13 shows typical adiabatic behaviour, the potential temperature being nearly

constant with height. Boundary layer is rather deep, and wind velocity smoothly varies with height above few tens of meters within which the wind profile is close to logarithmic shape.

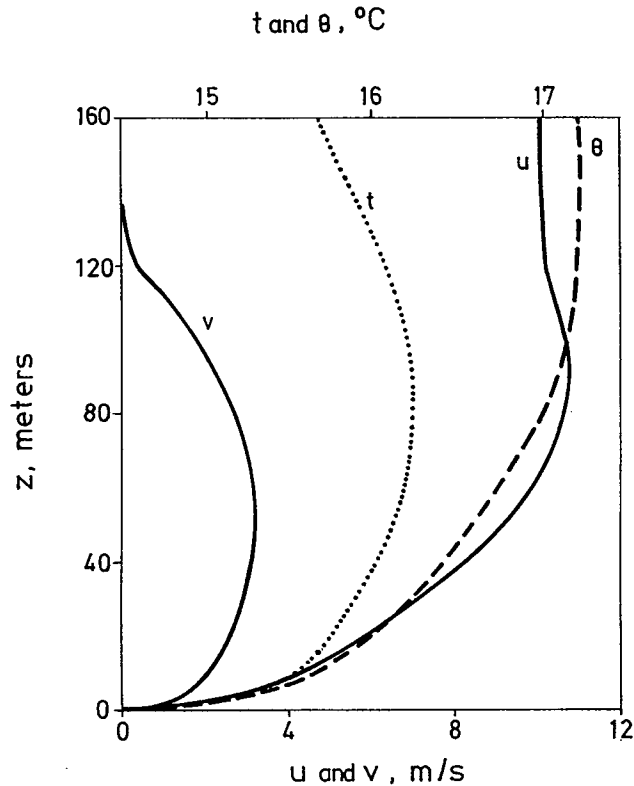


Figure 8.14. Simulated profiles of wind speed and temperature in the stable boundary layer with temperature inversion.

The velocity and temperature pattern in Figure 8.14 is quite different. Presented profiles correspond to the case when hydrostatic stability restricts the depth of the turbulent layer, and the effects of stratification on the velocity field are quite well pronounced. In the graph one can see the typical attributes of the SBL vertical structure: jet near the SBL top, wind direction strongly veering with height, low wind speed close to the surface. Still, compared to the previous plot, in the list of external parameters the only one was changed, here $T_2=15.2^\circ\text{C}$ ($z_2=2.0\text{m}$). Qualitatively calculated profiles are very similar to those presented in Figure 8.12 of Section 8.3.1 where basic features of SBL were discussed.

Acknowledgement

The author gratefully acknowledges the helpful co-operation with colleagues from the Laboratory of Fluid Mechanics of Ecole Centrale de Nantes where he started the work on this paper during his stay as an invited researcher.

References

- BATCHVAROVA, E. & GRYNING, S.-E. 1991 Applied model for the growth of the daytime mixed layer. *Boundary-Layer Met.* **56**, 261-274.
 BRUTSAERT, W. 1982 *Evaporation into the Atmosphere*. Reidel. 299pp.

city smoothly varies with
ose to logarithmic shape.



ire in the stable boundary

fferent. Presented profiles
of the turbulent layer, and
nounced. In the graph one
: near the SBL top, wind
ie surface. Still, compared
y one was changed, here
imilar to those presented in
scussed.

with colleagues from the
he started the work on this

th of the daytime mixed layer.

- CAUGHEY, S.J. & PALMER, S.G. 1991 Some aspects of turbulence structure through the depth of the convective boundary layer. *Quart. J. Roy. Met. Soc.* **105**, 811-827.
- CHORLEY, L.G., CAUGHEY, S.J. & READINGS, C.J. 1975 The development of the atmospheric boundary layer: three case studies. *Met. Mag.* **104**, 349-360.
- CLARKE, R.H., Dyer, A.J., Brook, R.R., Reid, D.G. & Troup, A.J. 1971 The Wangara experiment: Boundary layer data. Tech. Paper 19, Div. Meteor. Phys., CSIRO Australia, 363pp. [ISBN 0643 00648 6. NTIS N71-37838.]
- DEARDORFF, J.W. 1970a Preliminary results from numerical integration of the unstable boundary layer. *J. Atmos. Sci.* **27**, 1209-1211.
- DEARDORFF, J.W. 1970b Convective velocity and temperature scales for the unstable planetary boundary layer and for Raleigh convection. *J. Atmos. Sci.* **27**, 1211-1213.
- DEARDORFF, J.W. 1979 Prediction of convective mixed-layer entrainment for realistic capping inversion structure. *J. Atmos. Sci.* **36**, 424-436.
- DEARDORFF, J.W. & WILLIS, G.E. 1985 Further results from a laboratory model of the convective planetary boundary layer. *Boundary-Layer Met.* **32**, 205-236.
- DEARDORFF, J.W., WILLIS, G.E. & LILLY, D.K. 1969 Laboratory investigation of non-steady penetrative convection. *J. Fluid Mech.* **35**, 7-31.
- DEARDORFF, J.W., WILLIS, G.E. & STOCKTON, B.H. 1980 Laboratory studies of the entrainment zone of a convectively mixed layer. *J. Fluid Mech.* **100**, 41-64.
- DYER, A.J. 1974 A review of flux-profile relations. *Boundary-Layer Met.* **1**, 363-372.
- FERNANDO, H.J.S. 1991 Turbulent mixing in stratified fluids. *Annu. Rev. Fluid Mech.* **23**, 455-493.
- KANTHA, L.H. 1977: Note on the role of internal waves in thermocline erosion. In *Modelling and Predictions of the Upper Layer of the Ocean* (ed. E.B.Kraus), pp.173-177. Pergamon Press.
- LENSCHOW, D.H., WYNGAARD, J.C. & PENNEL, W.T. 1980 Mean-field and second-momentum budgets in a baroclinic, convective boundary layer. *J. Atmos. Sci.* **37**, 1313-1326.
- MASON, P.J. 1984 Large-eddy simulation for the convective atmospheric boundary layer. *J. Atmos. Sci.* **41**, 2052-2062.
- MOENG, C.-H. 1984 A large-eddy simulation for the study of planetary boundary layer turbulence. *J. Atmos. Sci.* **46**, 1492-1516.
- NELSON, E., STULL, R. & ELORANTA, E. 1989 A prognostic relationship for entrainment zone thickness. *J. Appl. Meteorol.* **28**, 885-903.
- NIEUWSTADT, F.T.M. 1990 Direct and large-eddy simulation of free convection. In *Proc. 9th Internat. Heat Transfer Conf., Jerusalem, August 19-24, 1990*, pp.37-47. Amer. Soc. Mech. Engrg., New York, Vol.I.
- SCHMIDT, H. & SCHUMANN, U. 1989 Coherent structures of the convective boundary layer derived from large-eddy simulations. *J. Fluid. Mech.* **200**, 511-562.
- SHAY, T.J. & GREGG, M.C. 1986 Convectively driven turbulent mixing in the upper ocean. *J. Phys. Oceanogr.* **16**, 1777-1798.
- STULL, R.B. 1976 Mixed-layer depth model based on turbulent energetics. *J. Atmos. Sci.* **33**, 1268-1278.
- STULL, R.B. 1988 *An Introduction to Boundary Layer Meteorology*. Kluwer Academic Publishers. 666pp.
- WILLIS, G.E. & DEARDORFF, J.W. 1974 A laboratory model of the unstable planetary boundary layer. *J. Atmos. Sci.* **31**, 1297-1307.
- THORPE, S.A. 1973 Turbulence in stably stratified fluids: a review of laboratory experiments. *Boundary-Layer Met.* **5**, 95-119.
- ZILITINKEVICH, S.S. 1972 On the determination of the height of the Ekman boundary layer. *Boundary-Layer Met.* **3**, 141-145.
- ZILITINKEVICH, S.S. 1975 Resistance laws and prediction equations for the depth of the planetary boundary layer. *J. Atmos. Sci.* **32**, 741-752.
- ZILITINKEVICH, S.S. 1989a Velocity profiles, the resistance law and the dissipation rate of mean flow kinetic energy in a neutrally and stably stratified planetary boundary layer. *Boundary-Layer Met.* **46**, 367-387.
- ZILITINKEVICH, S.S. 1989b The temperature profile and heat transfer law in a neutrally and stably stratified planetary boundary layer. *Boundary-Layer Met.* **49**, 1-5.
- ZILITINKEVICH, S.S. 1991 *Turbulent Penetrative Convection*. Avebury Technical. 179pp.

Address of the author

Dr. Evgeni Fedorovich
Institut für Hydrologie und Wasserwirtschaft
Universität Karlsruhe
76128 Karlsruhe, Deutschland
gg07@dkauni2.bitnet